Spatial Ordering of Organic and Inorganic Charge Centers in As-Made High-Silica Zeolites Determined by Multidimensional $\{^1H\} \rightarrow {}^2H$ CPMAS NMR Correlation Spectroscopy

Daniel F. Shantz and Raul F. Lobo*

Center for Catalytic Science and Technology, Department of Chemical Engineering, University of Delaware, Newark Delaware 19716

Received June 25, 1998. Revised Manuscript Received October 1, 1998

Evidence is presented for the spatial ordering of the organic and inorganic charge centers in the as-made tectosilicates nonasil, SSZ-23, and ZSM-12. This result is based on two-dimensional $^2H-\{^1H\}$ NMR correlation spectroscopy experiments, which show correlation between the silanol protons of the defect site and the *N*-methyl groups of the structure-directing agent. The two-dimensional NMR spectra for all samples suggest that the deuterons of the methyl groups adjacent to the organic charge center are preferentially ordered relative to the defect site. Experiments performed on a sample synthesized in D_2O are consistent with the interpretation of the two-dimensional NMR experiments. The results also suggest that Coloumbic organic−inorganic forces influence the location of the charge-compensating defect site in all-silica zeolites. Moreover, we suggest an additional role for certain cationic structure-directing agents in zeolite synthesis, controlling the location of T^{+3} atoms in the zeolite framework.

Introduction

Zeolites are microporous crystalline solids used extensively in heterogeneous catalysis, adsorption and separation of gases, and ion-exchange operations.[1] The framework composition (i.e. Si/Al ratio), framework topology, and number and identity of the extraframework cations determine the performance of a zeolite in adsorption or catalytic applications. Structural defects are also known to influence the catalytic and adsorptive properties of zeolites. Stacking faults, point defects, and hydroxyl nests are often present in industrial materials, and why they are present and how they affect physical properties remain unresolved.[2,3] It has been shown that as-made all-silica zeolites synthesized with cationic organic molecules contain charge-compensating defect sites.[4] All materials previously investigated have one siloxy and three silanol groups per organic cation, and ^1H NMR has shown that likely two of the silanols are engaged in strong hydrogen bonding with the siloxy group with an average SiOH···$^-$OSi distance of 2.7 Å.[4]

High-silica zeolites are usually synthesized using a quaternary ammonium cation, or structure-directing agent (SDA), that influences what product is obtained (i.e. framework topology) from synthesis.[5] While the size, geometry, and hydrophobicity of SDAs have been studied,[5,6] the nature of the organic−inorganic Coloumbic interactions in the synthesis gel and their role in the process of structure-direction are poorly understood. These ionic interactions may control the spatial distribution of framework defects or framework T^{+3} atoms (i.e. Al^{3+}, B^{3+}, Fe^{3+} etc.). Determining the role of ionic interactions in the structure-direction process should lead to a more rational design of zeolitic catalysts.

We have recently used variable temperature ^2H NMR spectroscopy to probe guest−host interactions in samples of as-made nonasil synthesized with trimethylalkylammonium compounds.[7] Our results show that none of the SDAs isotropically reorient in the nonasil cage, in contrast to nonasil samples made with the electrically

* Corresponding author. Phone: (302) 831-1261. Fax: (302) 831-2085. E-mail: lobo@che.udel.edu.

(1) (a) Barrer, R. M. *Hydrothermal Chemistry of Zeolites*; Academic Press: London, 1982. (b) Breck, D. W. *Zeolite Molecular Sieves*; Wiley: New York, 1974.

(2) (a) Chester, A. W.; Chum, Y. F.; Dessau, K. M.; Kerr, G. T.; Kresge, C. T. *J. Chem. Soc., Chem. Commun.* **1985**, 289. (b) Newsam, J. M.; Treacy, M. M. J.; Koetsier, W. T.; DeGruyter, C. B. *Proc. R. Soc. London A* **1988**, *420*, 375. (c) Englhardt, G.; Lohse, U.; Samoson, A.; Magi, M.; Tarmak, M.; Lippma, E. *Zeolites* **1982**, *2*, 59.

(3) (a) Dutartre, R.; de Menorval, L. C.; Direnzo, F.; McQueen, D.; Fajula, F.; Schulz, P. *Microporous Mater.* **1996**, *6*, 311. (b) Siantar, D. P.; Millman, W. S.; Fripiat, J. J. *Zeolites* **1995**, *15*, 556. (c) Dessau, R. M.; Smith, K. D.; Kerr, G. T.; Woolery, G. L.; Alemany, L. B. *J. Catal.* **1984**, *104*, 484.

(4) Koller, H.; Lobo, R. F.; Burkett, S. L.; Davis, M. E. *J. Phys. Chem.* **1995**, *99*, 12588.

(5) (a) Gies, H.; Marler, B. *Zeolites* **1992**, *12*, 42. (b) Lobo, R. F.; Zones, S. I.; Davis, M. E. *J. Inclusion Phenom. Mol. Recognit. Chem.* **1995**, *21*, 47. (c) Zones, S. I.; Nakagawa, Y.; Yuen, L. T.; Harris, T. V. *J. Am. Chem. Soc.* **1996**, *118*, 7558. (d) Yoshikawa, M.; Davis, M. E.; Zones, S. I. *Microporous Mater.* **1997**, *11*, 137. (e) Behrens, P.; Panz, C.; Hufnagel, V.; Lindlar, B.; Freyhardt, C. C.; van de Goor, G. *Solid State Ionics* **1997**, *101*, 229. (f) Balkus, K. J., Jr.; Gabrielov, A. G.; Shepelev, S. *Microporous Mater.* **1995**, *3*, 489. (g) van de Goor, G.; Freyhardt, C. C.; Behrens, P. *Z. Anorg. Allg. Chem.* **1995**, *621*, 311.

(6) (a) Burkett, S. L.; Davis, M. E. *J. Phys. Chem.* **1994**, *98*, 4647. (b) Kubota, Y.; Helmkamp, M. M.; Zones, S. I.; Davis, M. E. *Microporous Mater.* **1993**, *6*, 213. (c) Tsuji, K.; Davis, M. E. *Microporous Mater.* **1997**, *11*, 53. (d) Burkett, S. L.; Davis, M. E. *Chem. Mater.* **1995**, *7*, 1453. (e) Lewis, D. W.; Catlow, C. R. A.; Thomas, J. M. *J. Chem. Soc., Faraday Discuss.* **1997**, *106*, 451. (f) Cox, P. A.; Casci, J. L.; Stevens, A. P. *J. Chem. Soc., Faraday Discuss.* **1997**, *106*, 473.

(7) Shantz, D. F.; Lobo, R. F. *J. Phys. Chem. B* **1998**, *102*, 2339.

10.1021/cm9804517 CCC: $15.00
Published on Web 11/13/1998

neutral 2-aminopentane.[8] These results confirm the presence of strong Coloumbic forces between the cationic SDA and the defect site in the zeolite framework that cannot be overcome with the thermal energy available at temperatures of at least 370 K. The presence of strong organic−inorganic Coloumbic forces suggests that the charge center on the SDA could be spatially correlated to the charge-compensating defect in the zeolite framework. Here, using two-dimensional NMR correlation spectroscopy, we study this spatial correlation issue for the three all-silica tectosilicates nonasil (NON), SSZ-23, and ZSM-12 (MTW).

Nonasil[9] is a clathrasil, a class of natural and synthetic silicates whose structures are comprised of cages, as compared to zeolites, which have a one- or multidimensional open pore structure. The SDA used in synthesis is located in the largest cage of nonasil: an eicosahedra ($[5^8 6^{12}]$) with a free volume of approximately 290 Å^3. The highest topological symmetry of the nonasil framework is the orthorhombic space group *Fmmm*, though the symmetry of the as-made material changes depending on the SDA used.[7]

SSZ-23[10] is a zeolite with an unusual framework topology that is comprised of large cages connected by seven- and nine-membered rings.[11] SSZ-23 is synthesized using *N*,*N*,*N*-trimethyl-1-adamantammonium hydroxide as the structure-directing agent. The material can be made in an all-silica form as well as in the presence of a small amount of aluminum (Si/Al > 50).

ZSM-12 (MTW) is a large-pore zeolite with a one-dimensional elliptical pore architecture with dimensions of approximately 5.5 × 5.9 Å.[12,13] ZSM-12 can be synthesized using a variety of SDAs including tetraethylammonium hydroxide,[12] 4,4′-trimethylenebis(1,1′-dimethylpiperidinium) dihydroxide,[14a] *N*,*N*,*N*-trimethylbenzylammonium hydroxide,[14b] and *N*,*N*-dimethyldibenzylammonium hydroxide.[14c] ZSM-12 is also one of the few all-silica zeolites that can be made in the absence of alkali cations.[15] Due to its large pore structure, ZSM-12 has been the focus of numerous catalytic studies.[16]

Solid-state ^{2}H NMR spectroscopy is a useful tool for studying the dynamics of organic solids, including organic molecules occluded in microporous materials.[17] Deuterium has a nuclear spin $I = 1$, a static quadrupole coupling constant (QCC) between 150 and 200 kHz, and is an experimentally convenient quadrupolar nucleus because the quadrupolar interaction dominates other interactions such as dipole−dipole coupling and chemical shift anisotropy. ^{2}H NMR has been used by several research groups to study guest−host interactions in zeolites.[18] Magic-angle spinning ^{2}H NMR has also been shown to be a useful technique for studying the dynamics of organic molecules.[19] Instead of the powder pattern obtained from traditional static quadrupole echo experiments, sharp spinning sidebands are observed at integer multiples of the rotor frequency from the isotropic chemical shift. The number and relative intensities of the sidebands allow the determination of the QCC and asymmetry parameter. This technique results in a dramatic improvement in signal-to-noise and has even been employed to study deuterium in samples at natural abundance.[20]

Cross-polarization magic-angle spinning (CPMAS) experiments have enabled the routine study of naturally dilute nuclei such as ^{13}C and ^{29}Si with excellent spectral resolution.[21] The basic cross-polarization experiment consists of irradiating an abundant nucleus (i.e. ^{1}H) and spin-locking its magnetization in the *xy* plane of the laboratory frame. The dilute nucleus (i.e. ^{13}C) is then irradiated with a magnetic field B_1 such that the Hartmann−Hahn matching condition (for MAS) is satisfied,

$$\gamma_I B_{1I} = \gamma_S B_{1S} \pm n\omega_R \qquad n = 1, 2,...$$

with ω_R being 2π times the spinning rate. The theoretical maximum improvement in signal intensity for the dilute nucleus is γ_I/γ_S. The primary advantages of cross-polarization are the improvement in signal-to-noise for the dilute nucleus (i.e. ^{13}C) and the reduction in time between scans as the spin−lattice (T_1) relaxation time of ^{1}H is usually smaller than for dilute nuclei such as ^{13}C and ^{29}Si. The theory of cross-polarization between two spin $I = {}^1/_2$ nuclei is well-developed for both stationary and spinning samples.[21,22] The mechanism of magnetization transfer utilized in cross-polarization is dipole−dipole coupling between nuclei, which is

(8) Gies, H. In *Inclusion Compounds*; Atwood, J. L., Davies, J. E. D., MacNicol, D. D., Eds.; Oxford: New York, 1991; Vol. 5 (Inorganic and Physcial Aspects of Inclusion).

(9) Marler, B.; Dehnbostel, N.; Eulert, H. H.; Gies, H.; Liebau, F. *J. Inclusion Phenom.* **1986**, *4*, 339.

(10) Zones, S. I.; Innes, R. A. U.S. Patent 4,859, 442, 1989.

(11) Camblor, M. A.; Díaz-Cabañas, M. J.; Perez-Pariente, J.; Teat, S. J.; Clegg, W.; Shannon, I. J.; Lightfoot, P.; Wright, P. A.; Morris, R. E. *Angew. Chem., Int. Ed. Eng.* **1998**, *37*, 2122.

(12) Rosinski, E. J.; Rubin, M. K. U.S. Patent 3,832,449, 1974.

(13) Fyfe, C. A.; Gies, H.; Kokotailo, G. T.; Marler, B.; Cox, D. E. *J. Phys. Chem.* **1990**, *94*, 3718.

(14) (a) Valyocsik, E. W. U.S. Patent 4,593,193, 1985. (b) Rubin, M. K. U.S. Patent 4,585,637, 1985. (c) Rubin, M. K. U.S. Patent 4,-636,373, 1987.

(15) Goepper, M.; Li, H. X.; Davis, M. E. *J. Chem. Soc., Chem. Commun.* **1992**, 1665.

(16) (a) Chiche, B. H.; Dutartre, R.; Direnzo, F.; Fajula, F.; Katovic, A.; Regina, A.; Giordano, G. *Catal. Lett.* **1995**, *31*, 359. (b) Pu, S. B.; Inui, T. *Appl. Catal. A.* **1996**, *146*, 305. (c) Vogt, A.; Kouwenhoven, H. W.; Prins, R. *Appl. Catal. A.* **1995**, *123*, 37. (d) Reddy, K. S. N.; Rao, B. S.; Shiralkar, V. P. *Appl. Catal. A.* **1995**, *121*, 191.

(17) (a) Schmidt-Rohr, K.; Spiess, H. W. *Multidimensional Solid-State NMR and Polymers*; Academic: London, 1994. (b) Spiess, H. W. *Chem. Rev.* **1991**, *91*, 1321. (c) Vold, R. R. In *Nuclear Magnetic Resonance Probes of Molecular Dynamics*; Tycko, R., Ed.; Kluwer: London, 1994; Vol. 8 (Understanding Chemical Reactivity).

(18) (a) Burmeister, R.; Schwarz, H.; Boddenberg, B. *Ber. Bunsen-Ges. Phys. Chem.* **1989**, *93*, 1309. (b) Zibrowius, B.; Caro, J.; Pfeiffer, H. *J. Chem. Soc., Faraday Trans.* **1988**, *84*, 2347. (c) Bull, L. M.; Henson, N. J.; Cheetham, A. K.; Newsman, J. M.; Heyes, S. J. *J. Phys. Chem.* **1993**, *97*, 11776. (d) Bull, L. M.; Cheetham, A. K.; Powell, B. M.; Ripmeester, J. A.; Ratcliffe, C. I. *J. Am. Chem. Soc.* **1995**, *117*, 4328. (e) Sousa-Gonçlaves, J. A.; Portsmouth, R. L.; Alexander, P.; Gladden, L. F. *J. Phys. Chem.* **1995**, *99*, 3317. (f) Auerbach, S. M.; Bull, L. M.; Henson, N. J.; Metiu, H. I.; Cheetham, A. K. *J. Phys. Chem.* **1996**, *100*, 5923. (g) Vitale, G.; Bull, L. M.; Morris, R. E.; Cheetham, A. K.; Toby, B. H.; Coe, C. G.; MacDougall, J. E. *J. Phys. Chem.* **1995**, *99*, 16087. (h) Eckman, R.; Vega, A. J. *J. Am. Chem. Soc.* **1983**, *105*, 4841. (i) Eckman, R.; Vega, A. J. *J. Phys. Chem.* **1986**, *90*, 4679. (j) Kustanovich, I.; Fraenkel, D.; Luz, Z.; Vega, S.; Zimmernan, H. *J. Phys. Chem.* **1988**, *92*, 4134. (k) Vega, A. J.; Luz, Z. *Zeolites* **1988**, *8*, 19. (l) Kustanovich, I.; Luz, Z.; Vega, S.; Vega, A. J. *J. Phys. Chem.* **1990**, *90*, 3138.

(19) (a) Kristensen, J. H.; Bildsøe, H.; Jakobsen, H. J.; Nielsen, N. C. *J. Magn. Reson.* **1991**, *92*, 443. (b) Vega, S.; Weintraub, O. *Solid State Nucl. Magn. Reson.* **1995**, *4*, 341. (c) Kristensen, J. H.; Bildsøe, H.; Jakobsen, H. J.; Nielsen, N. C. *J. Magn. Reson.* **1992**, *100*, 437.

(20) Poupko, R.; Olender, Z.; Reichert, D.; Luz, Z. *J. Magn. Reson. A* **1994**, *104*, 113.

(21) Stejskal, E. O.; Schaefer, J.; Waugh, J. S. *J. Magn. Reson.* **1977**, *28*, 105.

proportional to the magnitude of the dipolar coupling constant ($\propto r^{-3}$).

Extending this technique to quadrupolar nuclei ($I > {}^1/_2$) is complicated by the quadrupole interaction. Both experimental and theoretical investigations of cross-polarization from a spin $I = {}^1/_2$ nucleus to a half-integer quadrupolar nucleus (i.e. $I = {}^3/_2$ or ${}^5/_2$) are available.[23] In this work, we focus on cross-polarization from a spin $I = {}^1/_2$ nucleus (^{1}H) to a spin $I = 1$ nucleus (^{2}H) to probe the relative spatial proximity of the SDA and the defect site in as-made zeolites. The possibility of ^{2}H−{^{1}H} CPMAS was first demonstrated over 15 years ago,[24] and subsequent works have investigated ^{2}H−{^{1}H} CPMAS using model compounds.[25] Zumbulyadis has studied miscibility in polymer blends using ^{2}H−{^{1}H} CPMAS NMR,[26] and we recently used two-dimensional ^{2}H−{^{1}H} heteronuclear correlation (HETCOR) spectroscopy experiments on zeolitic systems using cross-polarization as the mixing mechanism.[27] Because of electric field gradient (EFG) modulations in the *z* direction due to sample spinning, the quadrupole interaction often results in inefficient spin-locking of the quadrupolar nuclei and subsequently poor cross-polarization.[23,24] This problem has been studied for CPMAS between ^{1}H and a spin $I = 1$ nucleus with relatively small QCCs ($\omega_Q/2\pi < 200$ kHz) such as deuterium.[25b] Deuterons which have large QCCs have different spin-locking and cross-polarization behavior than spin $I = {}^1/_2$ nuclei; however, in the limit of strong radio-frequency (rf) fields and small quadrupole coupling constants ($\omega_{1S} \gg \omega_Q$) the cross-polarization and spin-locking behavior of spin $I = 1$ nuclei are similar to spin $I = {}^1/_2$ nuclei.[25b]

Fyfe and co-workers were the first to use multidimensional spectroscopy to study zeolitic materials.[28] Multidimensional correlation spectroscopy experiments involving cross-polarization were used to study the three-dimensional connectivity of VPI-5, $AlPO_4$-8, and zeolites A, X, Y, and Ω.[28] Vega used two-dimensional cross-polarization NMR experiments to study the spatial siting of silanol groups in zeolites A and *ρ*.[29]

Here we study the spatial ordering of the organic and inorganic charge centers in as-made all-silica zeolites using two-dimensional correlation NMR spectroscopy and samples synthesized with selectively labeled SDAs. The all-silica zeolites studied in this work have a ^{1}H NMR resonance between 9.8 and 10.6 ppm due to the framework charge-compensating defect site, well resolved from the resonances of the organic SDA. By selective deuteration of the SDA, we can use ^{2}H−{^{1}H} two-dimensional correlation spectroscopy with cross-polarization to probe the orientation of the SDA relative to the framework defect site. Due to the strong spatial dependence on the rate of cross-polarization ($\propto r^{-6}$), ^{2}H−{^{1}H} CPMAS should be a useful tool for qualitatively probing the spatial ordering of the charge centers in as-made all-silica zeolites. Also, deuteration of the SDA at the *N*-methyl position chemically simplifies the system such that there are two types of protons (defect silanols and organic protons of the substituent alkyl group) and one type of deuteron. This facilitates the use and interpretation of heteronuclear correlation spectroscopy experiments, where the spatial proximities of different segments of the SDA and the defect site can be qualitatively studied by observing at what chemical shift value the ^{2}H resonance is observed in the ^{1}H frequency dimension. If the deuterated methyl groups are in close spatial proximity to the defect silanol groups, then it should be possible to transfer magnetization from the silanol protons to the deuterons of the methyl groups. This magnetization transfer is manifested in the two-dimensional correlation spectrum as a resonance at approximately 10 ppm in the ^{1}H frequency dimension. The correlation spectra for all samples indicate that magnetization is transferred from the silanol groups to the methyl deuterons. Experiments performed on a nonasil sample prepared in D_2O with a labeled SDA suggest that the methyl deuterons are closer to the defect sites than the substituent alkyl group, consistent with the interpretation of the two-dimensional HETCOR experiments. The results indicate that an additional role of the SDA during synthesis is to influence the location of defect sites in all-silica zeolites. This work also gives additional support to the importance of organic−inorganic Coloumbic interactions during zeolite synthesis and the process of structure-direction. This raises the possibility of changing the distribution of catalytic sites in a zeolite on the basis of the charge distribution of the SDA.

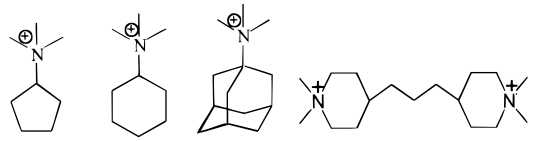

I **II** **III** **IV**

Figure 1. Organic molecules used in zeolite synthesis.

Experimental Section

Sample Preparation. Figure 1 shows the organic SDAs used in the synthesis of nonasil (**I** and **II**), SSZ-23 (**III**), and ZSM-12 (**IV**). The synthesis of nonasil using selectively deuterated SDAs has been described previously.[7] The nonasil samples investigated here were made with *N*,*N*,*N*-trimethylcyclopentylammonium hydroxide-d_9 (TMC5-d_9−NON) and *N*,*N*,*N*-trimethylcyclohexylammonium hydroxide-d_9 (TMC6-d_9−NON) synthesized in H_2O and D_2O.

Synthesis of *N*,*N*,*N*-Trimethyl-1-adamantammonium Hydroxide. A 10 g portion of 1-adamantanamine (99%, Aldrich) is added to 60 mL of *N*,*N*-dimethylformamide (ACS Reagent, Fisher) and 37 mL of tributylamine (99%, Aldrich). The solution is immersed in an ice bath before the dropwise

(22) (a) Mehring, M. *Principles of High-Resolution NMR in Solids*, 2nd ed.; Springer-Verlag: Berlin, 1983. (b) Stejskal, E. O. *High-Resolution NMR in the Solid State: Fundamentals of CP/MAS*; Oxford: New York, 1994. (c) Meier, H. In *Advances in Magnetic and Optical Resonance, Vol 18*; Warren, W. S., Ed.; Academic: San Diego, 1994.

(23) (a) Vega, A. J. *J. Magn. Reson.* **1992**, *96*, 50. (b) Harris, R. K.; Nesbitt, G. J. *J. Magn. Reson.* **1988**, *78*, 245. (c) Walter, T. H.; Turner, W. L.; Oldfield, E. *J. Magn. Reson.* **1988**, *76*, 106. (d) Vega, A. J. *Solid State Nucl. Magn. Reson.* **1992**, *1*, 17. (e) DePaul, S. M.; Ernst, M.; Shore, J. S.; Stebbins, J. F.; Pines, A. *J. Phys. Chem. B* **1997**, *101*, 3240.

(24) Müller, L. *Chem. Phys.* **1981**, *61*, 235.

(25) (a) Potrzebowski, M. J.; Wasiak, J.; Ciesielski, W.; Klinowski, J. *J. Magn. Reson. A* **1995**, *114*, 70. (b) Marks, D.; Zumbulyadis, N.; Vega, S. *J. Magn. Reson. A* **1996**, *122*, 16.

(26) (a) Zumbulyadis, N.; O'Reilly, J. M. *J. Am. Chem. Soc.* **1993**, *115*, 4407. (b) Zumbulyadis, N.; Landry, M.; Russell, T. P. *Macromolecules* **1996**, *29*, 2201.

(27) Shantz, D. F.; Lobo R. F. *J. Am. Chem. Soc.* **1998**, *120*, 2482.

(28) See Fyfe, C. A.; Mueller, K. T.; Kokotailo, G. T. In *NMR Techniques in Catalysis*; Bell, A. T., Pines, A., Eds.; Marcel Dekker: New York, 1994, and references therein.

(29) Vega, A. J. *J. Am. Chem. Soc.* **1988**, *110*, 1049.

Table 1. Summary of the Gel Compositions and Temperatures Used for Zeolite Syntheses

sample	molar ratios in the synthesis gel	synthesis temp, K
TMC5−NON	1:0.15:0.10:45 SiO_2:R^+OH^-:NaOH:H_2O	433
TMC6−NON	1:0.15:0.125:45 SiO_2:R^+OH^-:NaOH:H_2O	443
MTW	1:0.06:0.30:32 SiO_2:$R^{2+}(OH^-)_2$:NaOH:H_2O	433
SSZ-23	1:0.27:0.01:40 SiO_2:R^+OH^-:KOH:H_2O	433

addition of 13 mL of iodomethane. The solution is stirred for 3 h in the ice bath and then removed and kept at 5 °C overnight. The solids are collected by filtration, rinsed with acetone, and dried (yield of approximately 60%). The iodide form is converted to the hydroxide form using a 5-fold excess of ion-exchange resin (IONAC NA-38, OH^- form). The conversion of the iodide to hydroxide is greater than 95% on the basis of titration of the resultant solution. The ^{13}C NMR data for the iodide salt in $CDCl_3$ are δ = 73.0, 48.7, 35.0, 34.9, and 29.2 ppm.

4,4′-Trimethylenebis(1,1′-dimethylpiperidinium) Dihydroxide. A 13.5 mL (50 mmol) portion of 4,4′-trimethylenebis(1-methylpiperidine) (99%, Aldrich) is added to 300 mL of acetone (99% ACS reagent, Fisher), 28 mL of methyl iodide (99%, Aldrich) is added dropwise, and the solution is allowed to react for 14 h in the absence of light at room temperature. The resulting solids are filtered, rinsed with ether, and dried. The crude iodide salt is recrystallized from hot methanol (∼85% yield). For ion exchange a 5-fold excess of ion-exchange resin is used, and the conversion of the iodide to hydroxide is checked as above. The ^{13}C NMR data for the iodide salt in D_2O are δ = 65.0, 58.3, 49.2, 36.8, 34.4, 28.4, 25.0 ppm.

Structure-directing agents with selectively deuterated methyl groups were made using CD_3I (99+% D, Cambridge Isotopes). Complete deuteration was verified by solution ^1H NMR. The MTW-d_{12} SDA was made from 4,4′-trimethylenebis(piperidine) (98%, Aldrich). Samples were also prepared using D_2O (99.9% D, Aldrich) as the solvent. The ion-exchange, titration, and synthesis mixture preparation were done in a glovebag under an argon atmosphere, using silver(I) oxide (99%, Aldrich) in a 5-fold excess to perform the ion-conversion from the iodide to the hydroxide form.

Zeolite Synthesis. Table 1 lists the stoichiometry used for the syntheses of the three zeolites. The procedure for a typical synthesis of all-silica ZSM-12 is as follows: 1.8 g of Cab-O-Sil M5 is mixed with 9 mL of 0.2 M 4,4′-trimethylenebis(1,1′-dimethylpiperidinium) dihydroxide, 8 mL of deionized water, and 0.36 g of ground sodium hydroxide (95%, Aldrich). The solution is stirred for approximately 2 h, until a liquidlike gel is obtained. The solution is then sealed in two 23 mL Teflon-lined Parr autoclaves and heated at 160 °C for 7 days under autogenous pressure and static conditions. After the synthesis period the autoclaves are cooled and the solids are collected by filtration, washed several times with deionized water, and dried overnight at 80 °C.

The procedure for a typical synthesis of all-silica SSZ-23 is as follows: 0.88 g of Cab-O-Sil M5 is mixed with 23 mL of 0.17 M *N,N,N*-trimethyl-1-adamantammonium hydroxide and 0.084 g of KOH (85%, Aldrich). The solution is mixed for 30 min, until a clear liquidlike gel is obtained. The solution is then sealed in two 23 mL Teflon-line Parr autoclaves and heated at 160 °C for 7 days at autogenous pressure and static conditions. After the synthesis period the autoclaves are cooled and the solids are treated as above. Seeding is only used in the case of the all-silica synthesis of SSZ-23, where 0.05 wt % of as-made SSZ-23 (Si/Al ∼ 110) is used as a seed material.

Analytical. Powder X-ray diffraction (XRD) is performed on samples using a Phillips 3000 X'Pert System with Cu Kα radiation. The patterns used for indexing are collected from 4° to 50° 2θ using the step scan mode, a 0.02° step size, and 15 s count time per step. The peak deconvolution is carried out using the Phillips package ProFit, and refinement of the unit cell parameters is done using the program Lapod.[30] Scanning electron microscopy (SEM) is performed using a JEOL 850 operating at 10 kV. TGA measurements are performed using a Cahn TG-121 microbalance with a heating rate of 2 °C/min from room temperature to 650 °C. Molecular modeling is performed using Cerius^2 3.2.[31] Structures used for molecular modeling are obtained with the Minimizer function in Cerius using the default parameters.

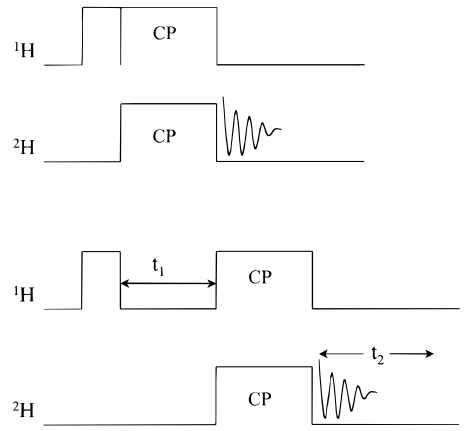

Figure 2. Pulse sequences used for the (a) one-dimensional and (b) two-dimensional $^2H-\{^1H\}$ CPMAS experiments.

Solution ^{13}C and ^1H NMR spectra are measured on a Bruker AC 250 spectrometer at 62.26 and 250 MHz with the chemical shifts referenced to tetramethylsilane. ^{29}Si, ^{13}C, ^1H, and ^2H solid-state NMR spectra are measured on a Bruker MSL 300 spectrometer at 59.63, 75.47, 300.13, and 46.07 MHz, respectively. Chemical shifts for the ^{29}Si, ^{13}C, and ^1H spectra are referenced to tetramethylsilane. Chemical shifts quoted for ^2H spectra in ppm are referenced to D_2O (δ_{D_2O} = 0). ^{29}Si MAS NMR spectra are acquired using a 7 mm probe with ZrO_2 rotors, a spin rate of 3 kHz, a 4 μs 60° pulse, high-power proton decoupling, and a 100 s recycle delay to avoid relaxation effects in the signal intensities. The structural integrity of the structure-directing agents inside the as-made samples is verified by ^{13}C CPMAS NMR using a contact time of 5 ms, a spin rate of 3 kHz, a 90° ^1H pulse of 6 μs, and high-power proton decoupling. ^1H MAS spectra are acquired using a 4 mm probe with ZrO_2 rotors, a spin rate of 9 kHz, a 20 s recycle delay, and a 5 μs 90° pulse. ^2H magic-angle spinning experiments are performed using a 4 mm probe with ZrO_2 rotors, a spin rate of 9 kHz, a 5 μs 90° pulse, and recycle delays between 1 and 5 s. ^{29}Si, ^1H, and ^2H MAS NMR line shape simulations were performed using NUTS from Acorn NMR.

Figure 2 shows the one- and two-dimensional $^2H-\{^1H\}$ CPMAS pulse sequences. Unless noted, $^2H-\{^1H\}$ CPMAS spectra are acquired with a ^2H rf field of 50 kHz (5 μs 90° pulse) and a spin rate of 9 kHz, and the ^1H rf field was varied to find the optimal Hartmann−Hahn matching condition. The Hartmann−Hahn matching condition is optimized on each sample by acquiring CPMAS spectra using a 3 ms contact time. The magnitude of the ^1H rf field is obtained by determining the 90° pulse length on a sample of adamantane using the same power settings. The optimum Hartmann−Hahn match was found using a proton rf field of 41 kHz (∼6.15 μs 90°). The optimum Hartmann−Hahn match for a $I = {}^1/_2$ nucleus often differs from the static case ($\gamma_I B_{1I} = \gamma_S B_{1S}$) by an integer multiple of the rotor frequency.[29] No proton decoupling is employed in either the one- or two-dimensional cross-polarization experiments. The relative intensity of the cross-polarization spectrum quoted (i.e. $S_{CP}/S_{\pi/2}$) is obtained using a 3 ms contact time and 32 scans for both CPMAS and the one-pulse

(30) Lapod, written by J. Ian Langford, School of Physics and Space Research, Univerisity of Birmingham B15 2TT UK.

(31) Cerius^{2}3.2. Product of MSI and Biosym.

MAS spectra, and in both cases, recycle delays sufficient for full relaxation were used. To verify that the ^{2}H CPMAS signal observed is not an artifact, null spectra were collected using the cross-polarization pulse sequence with the ^{1}H rf turned off. No signal is observed in the absence of the ^{1}H rf field.

Two-dimensional correlation spectroscopy experiments are performed using a 200 μs contact time (unless noted) with an eight-step phase-cycling list. Sixty-four experiments are performed, the F2 (^{2}H) dimension contains 4096 data points, the F1 (^{1}H) dimension is zero-filled from 128 to 256 data points, and a 20 kHz sweepwidth is used in the F1 (^{1}H) dimension. The two-dimensional Fourier transform is done in the power mode. ^{1}H T_1 experiments are performed on each sample to ensure that the recycle delay used is sufficient to avoid saturation effects, and efficient spin-locking of the protons is verified by performing $T_{1\rho}$ measurements. Proton spin-diffusion is monitored by two-dimensional ^{1}H spectroscopy using a ($\pi/2-t_1-$spin lock$-t_2$) pulse sequence.[29] Using a spin-lock time of 200 μs, only a small amount of spin-diffusion between the organic and silanol protons is observed.

Extension of the cross-polarization technique to multidimensional correlation spectroscopy requires determination of the optimal spin rate and rf field strengths for each individual sample. Minimizing proton spin-diffusion is essential, resulting in short (<500 μs) contact times. The spinning rate and the rf field strengths used are coupled due to the Hartmann−Hahn matching condition. Using high spin rates minimizes the number of sidebands in the ^{2}H CPMAS spectrum, improving the signal-to-noise and shortening the acquisition time in the two-dimensional experiments. However, the efficiency of cross-polarization is dependent on the spin rate, and higher spinning rates may result in less efficient cross-polarization. A detailed presentation of the physical and experimental parameters such as the proton homonuclear dipolar coupling, the quadrupole frequency, spin rate, and rf field strengths and how they affect these experiments can be found elsewhere.[32]

Results and Discussion

Material Characterization. Figure 3 shows typical XRD patterns for the three as-made materials. On the basis of XRD and scanning electron micrographs (not shown), all materials are highly crystalline and contain no impurities. The nonasil particles are nearly spherical and in all cases the crystals are larger than 1 μm.[7] The SSZ-23 crystals are spherical and are on average 5 μm in size, and the ZSM-12 samples are ellipsoidal with dimensions of approximately 2 μm.

Figure 4 shows the single-pulse ^{29}Si NMR spectrum of the three materials, and results of the line shape simulations are given in Table 2. In all spectra two lines (or group of lines) are observed: one is assigned to silicon atoms with one adjacent silanol or siloxy group (Q^3), and another is assigned to silicon atoms with four silicon atoms as nearest neighbors (Q^4) (where Q^n stands for $X_{4-n}Si[OSi]_n$, X = OH or O^-).[33] The Q^3/Q^4 ratio is directly related to the number of silanol groups in the zeolite framework. The number of lines used in the ^{29}Si NMR line shape simulations was chosen to optimize the agreement and do not represent crystallographically inequivelant sites. The Q^3/Q^4 ratios for NON, MTW, and SSZ-23 are 0.20 (TMC6−NON), 0.23 (TMC5−NON), 0.21, and 0.27, respectively. This corresponds to four Q^3 per N^+ for the nonasil and ZSM-12 samples. On the basis of TGA data for both the ZSM-12 and SSZ-23 samples, we also conclude that there are four Q^3 per N^+. The relative contribution of the surface silanol groups to the Q^3 line's intensity is negligible due to the small external surface area of these large crystals.

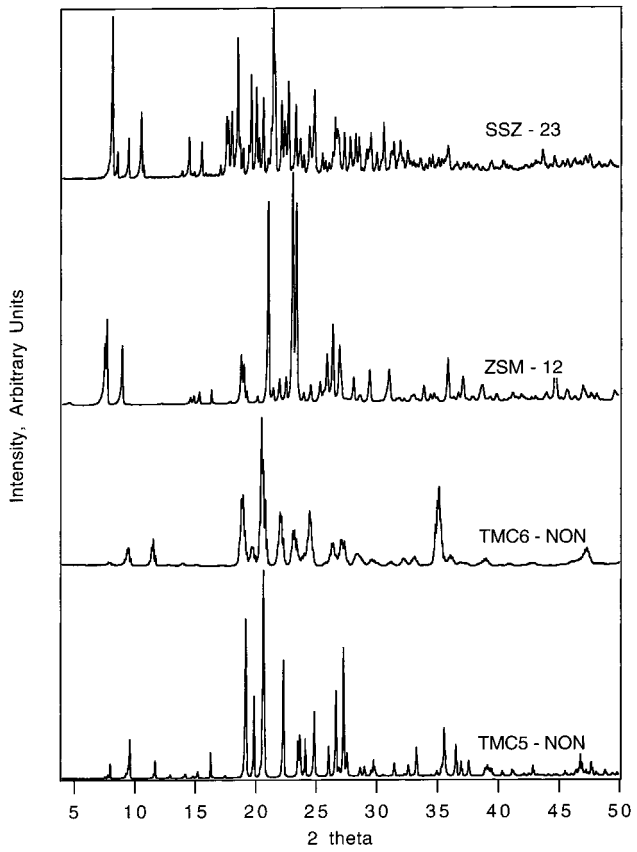

Figure 3. X-ray diffraction patterns of the as-made materials. The TMC5−NON unit cell parameters are $a_o = 22.15$ Å, $b_o = 15.14$ Å, $c_o = 13.69$ Å, $\alpha = \beta = \gamma = 90°$, and the as-made ZSM-12 unit cell parameters are $a_o = 24.88$ Å, $b_o = 5.00$ Å, $c_o = 24.31$ Å, $\alpha = \gamma = 90°$, $\beta = 107.7°$.

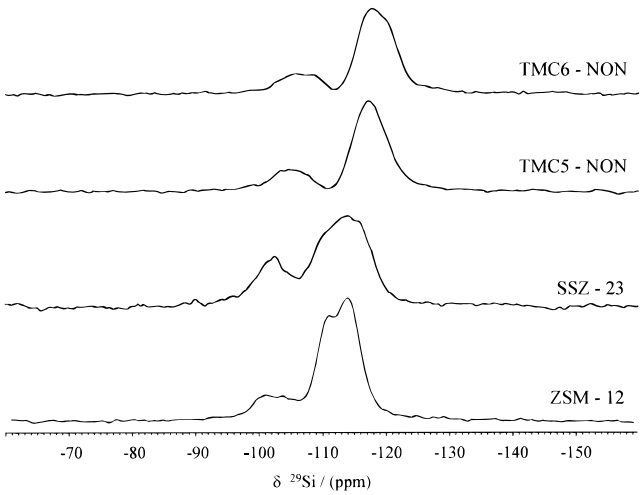

Figure 4. ^{29}Si NMR spectra of the as-made materials.

^{1}H NMR. Figure 5 shows the ^{1}H NMR spectra of samples made with selectively deuterated SDAs. All samples exhibit a strong resonance between 1 and 3 ppm due to the protons on the SDA, which is well-resolved from the resonances downfield ($\delta \geq 10$ ppm) due to the silanol groups in the defect sites. The nonasil samples have a broad line between 2 and 2.5 ppm assigned to the cyclic alkyl group protons and a signal at 5.8 ppm assigned to either water or silanol groups

(32) Shantz, D. F.; Lobo, R. F. Submitted to *J. Phys. Chem. B.*
(33) Engelhardt, G.; Michel, D. *High-Resolution Solid State NMR of Silicates and Zeolites*; Wiley: Chichester, 1987

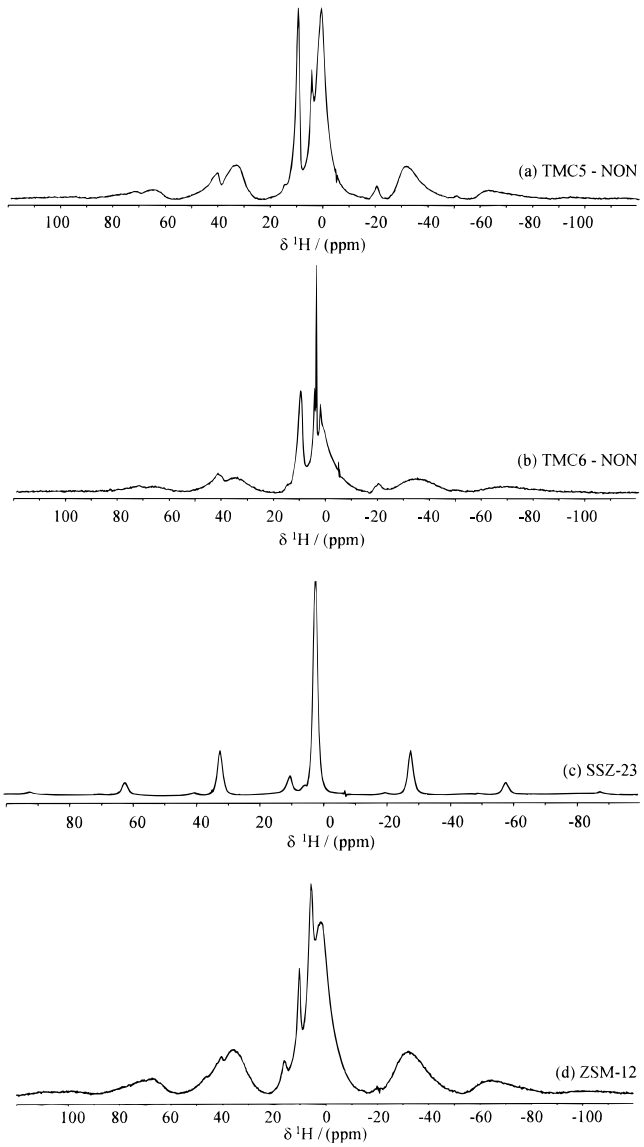

Figure 5. ^{1}H NMR spectra for (a) TMC5-d_9 nonasil, (b) TMC6-d_9 nonasil, (c) SSZ-23-d_9, and (d) ZSM-12-d_{12}.

Table 2. Summary of ^{29}Si MAS NMR Spectral Parameters

	Q^3		Q^4		
sample	chemical shift, δ (ppm)	relative intensity I	chemical shift, δ (ppm)	relative intensity I	Q^3/Q^4
TMC5−NON	−104.6	18.6	−117.3	81.4	0.23
TMC6−NON	−104.7	14.9	−116.9	35.8	0.20
	−108.6	2.1	−120.3	47.2	
MTW	−100.2	7.4	−110.3	26.7	0.21
	−103.9	9.7	−114.1	56.2	
SSZ-23	−101.8	21.2	−109.4	14.3	0.27
			−114.3	64.5	

not part of strong hydrogen bonds. The TMC6-d_9 nonasil sample has a signal at 3.1 ppm assigned to the methine proton on the alkyl ring and a sharp line at 4.8 ppm most likely due to water. The SSZ-23-d_9 sample has a line at 2.0 ppm assigned to the protons on the adamantane moiety and a line at 5.7 ppm, which is possibly due to silanol groups not associated with strong hydrogen bonds. The ZSM-12-d_{12} sample has a broad signal at 2.5 ppm assigned to the methylene protons on the SDA and a line at 5.8 ppm assigned to water and silanol groups in the defect sites not participating in hydrogen bonding. In work done with a sample of ZSM-5 synthesized with perdeuterated tetrapropylammonium hydroxide, Koller and co-workers observed a weak resonance at 6.5 ppm, and this was assigned to silanol groups in the defect site not participating in strong hydrogen bonding.[4] Results of inelastic neutron scattering experiments performed on the same sample[34] are consistent with the interpretation of the NMR data. Therefore, we tentatively assign the resonance between 5 and 6 ppm due to silanols groups in the defect not participating in strong hydrogen bonding with the siloxy group.

Table 3. ^{1}H NMR Downfield ($\delta \geq 10$ ppm) Resonances of Samples Made with Selectively Deuterated SDAs[a]

TMC5−NON		TMC6−NON		SSZ-23		MTW	
δ, ppm	d, Å	δ, ppm	d, Å	δ, ppm	d, Å	δ, ppm	d, Å
10.5	2.7	10.6	2.7	9.8	2.7	10.3	2.7
11.6	2.6	11.8	2.6	11.3	2.7	11.8	2.6
15.1	2.5	15.5	2.5			16.2	2.5

[a] The distances are for SiOH···OSi, are determined using a correlation given in ref 35, and are rounded to the nearest 0.1 Å.

Table 3 lists the chemical shift, relative intensity, and Si−OH···$^-$O−Si distance for the downfield ($\delta \geq 10$ ppm) resonances in the as-made materials. All samples have an asymmetric line between 9.8 and 10.7 ppm ("the line at 10 ppm") which can be deconvoluted into two lines. The nonasil and ZSM-12 samples exhibit a weaker additional line between 15.1 and 16.2 ppm ("the line at 15 ppm"). The resonance at 15 ppm is not observed for the nonasil samples made with fully protonated SDAs or the SSZ-23 sample and has not been reported previously.[4] Samples used in that work had fully protonated SDAs, except for the deuterated ZSM-5 sample that was made *without* sodium. We prepared a sample of TMC5-d_9 nonasil synthesized without sodium to determine if the alkali cations are responsible for the resonance at 15 ppm, which corresponds to a $d_{SiOH\cdots OSi}$ distance of approximately 2.5 Å.[35] There is no signal at 15 ppm for the nonasil sample made in the absence of sodium, indicating that the sodium cations are responsible for the resonance at 15 ppm. On the other hand, ^{29}Si NMR indicates that the sample made without sodium has approximately the same number of Q^3 groups as samples made with sodium. However, ^{29}Si NMR experiments may not be sensitive enough to detect small changes in the number of Q^3 groups present. One alternative is that the line at 15 ppm is due to defect sites with only one silanol group present instead of three. It is not possible from the available information to determine whether the line at 15 ppm is cation specific or if the cation is in spatial proximity to the defect. The origin of this resonance requires further investigation.

^{2}H NMR. Figure 6 shows the ^{2}H−{^{1}H} CPMAS spectra for TMC5-d_9 nonasil and ZSM-12-d_{12}. The ^{2}H−{^{1}H} CPMAS spectra of TMC6-d_9 nonasil and SSZ-23-d_9 (see the Supporting Information) are essentially identical to those of the TMC5-d_9 nonasil sample. The

(34) Lobo, R. F.; Eckert, J. Submitted to *Microporous Mater.*
(35) Eckert, H.; Yesinowski, J. P.; Silver, L. A.; Stolper, E. M. *J. Phys. Chem.* **1988,** *92,* 2055.

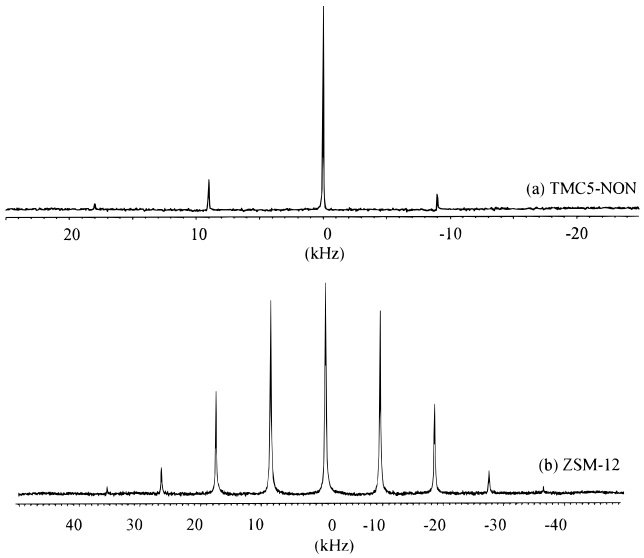

Figure 6. $^2H-\{^1H\}$ CPMAS spectra for (a) TMC5-d_9 nonasil and (b) ZSM-12-d_{12}. Thirty-two scans were acquired for (a) with a 3 ms contact time. Two hundred and fifty-six scans were acquired for (b) with a 2 ms contact time.

TMC5-d_9 and TMC6-d_9 nonasil samples have quadrupole coupling constants of 15.1 and 15.2 kHz, respectively.[7] The values are consistent with rapid rotations about the methyl groups' C_3 axes as well as the R−N bond axis, with some additional motion. The integrated spectral intensities of the ^2H CPMAS spectra are 70% (TMC5) and 60% (TMC6) of the single-pulse ^2H MAS spectrum. Simulation of the room-temperature static ^2H spectrum (see the Supporting Information) of SSZ-23 gives a quadrupole coupling constant of 13.0 kHz and an asymmetry parameter $\eta = 0.03$. The QCC value is consistent with a rapid internal rotation of the methyl groups and a rapid rotation along the R−N bond axis. There is an additional motion, since 13 kHz is lower than what would be expected (∼19 kHz) if only the two rotations are present. ^2H spin−lattice (T_1) relaxation experiments show that T_1 is anisotropic; thus, the additional motion leading to a further narrowing of the line shape has at least a 3-fold symmetry axis ($\eta \approx 0$), and the motion has discrete jumps (creating the T_1 anisotropy).[36] The integrated intensity of the $^2H-\{^1H\}$ CPMAS spectrum is 75% of the intensity of the single pulse ^2H MAS spectrum.

The QCC of the ZSM-12 sample is approximately 45 kHz. The static ^2H spectrum of the ZSM-12 sample does not exhibit the usual sharp features of a Pake doublet, indicating that the motion is in the intermediate motion regime (∼10^6 s^{-1}, see the Supporting Information). The signal intensity is weaker than would be expected as compared to samples with similar amounts of deuterium. A marked decrease in signal intensity is consistent with the motion being on the time scale of the ^2H NMR experiment.[37] The methyl group rotation has a low activation energy barrier (2−5 kJ/mol),[38] so it seems unlikely that the rotation rate is on the time scale of the NMR experiment. As a comparison, the static ^2H NMR spectrum of the neat SDA (Suporting Information) is a Pake doublet with a QCC of 51.5 kHz and $\eta = 0.03$. The increased asymmetry and decreased QCC of the ZSM-12 sample compared to the neat SDA suggests the presence of an additional motion. For example, a small angle rotation of the piperidinium moieties on the NMR time scale superimposed over the methyl group rotation could lead to the observed line shape. The observed line shape could also be due to packing effects (the SDAs are not isolated) and/or distortions of the electric field gradient around the deuteron. The SDAs in this sample are in close contact with each other, in contrast to the other materials studied here. This leads to two defect sites being in close proximity to each other since the pores are one-dimensional and the SDAs pack along the axis of the pore. Also, because the SDAs are close to each other there could be electrostatic repulsion due to neighboring charges, resulting in distortions of the EFG around the deuteron. Low-temperature ^2H NMR experiments on the sample (not shown) are consistent with the presence of an additional motion. In this sample the integrated spectral intensity of the ^2H CPMAS spectrum is 50% of the integrated intensity of the ^2H one-pulse MAS spectrum. The larger QCC leads to an effective decrease in the signal-to-noise ratio since the signal is spread into more sidebands. The proton homonuclear dipolar coupling is also more pronounced in this sample.

The theoretical maximum improvement in signal-to-noise for a $^2H-\{^1H\}$ cross-polarization experiment is $S_{CP}/S_{\pi/2} = \gamma^1_H/\gamma^2_H = 6.5$. The values we observe are much lower for three reasons: (1) for the nonasil and SSZ-23 samples the deuterons are undergoing two rapid rotations, (2) in all samples the deuterons are not dilute relative to the proton reservoir, and (3) the quadrupole interaction makes spin-locking and cross-polarization generally less efficient than in the spin $I = {}^1/_2$ case (this is most pronounced for the ZSM-12 sample). Nonetheless, it is possible to obtain a ^2H cross-polarization signal from all of the samples with a single scan if the Hartmann−Hahn match is optimized. In the case of the ZSM-12 sample, the reduced spectral intensity due to the molecular motion discussed above and reduced CP efficiency (larger QCC) lead to increased acquisition times in the two-dimensional experiments.

Multidimensional NMR. *Nonasil.* Two-dimensional heteronuclear correlation (HETCOR) experiments were performed to determine which protons in the samples are responsible for the magnetization transfer observed in the one-dimensional ^2H CPMAS spectrum. The two-dimensional spectrum of TMC5-d_9 nonasil is shown in Figure 7 and two resonances are observed, a line at 10.5 ppm and a line at 1.2 ppm. Due to the nature of cross-polarization, the relative intensities of the resonances are not quantitative. Molecular modeling[31] shows that the average distance from the methine proton to the *closest* methyl deuteron is between 1.9 and 2.2 Å, and the closest methylene protons on the cyclopentyl ring are approximately 2.3 Å from the closest methyl deuterons (the van der Waal's radius of hydrogen is approximately 1.25 Å).[39] The HETCOR results show that the silanol groups are involved in cross-polarization to the methyl deuterons at a contact time

(36) Torchia, D. A.; Szabo, A. *J. Magn. Reson.* **1982**, *49*, 107.
(37) Spiess, H. W.; Sillescu, H. *J. Magn. Reson.* **1981**, *42*, 381.
(38) Sidhu, P. S.; Bell, J.; Penner, G. H.; Jeffrey, K. R. *Can. J. Chem.* **1995**, *73*, 2196.
(39) Bondi, A. *J. Phys. Chem.* **1964**, *68*, 441.

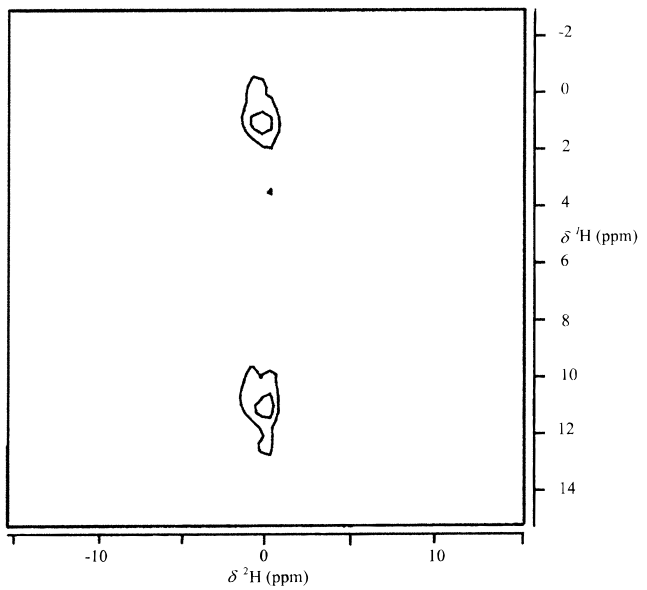

Figure 7. Two-dimensional $^2H-\{^1H\}$ CPMAS spectrum for TMC5-d_9 nonasil with a 200 μs contact time. Sixty-four scans were acquired for each experiment, a 20 Hz line broadening was used in both dimensions, and the acquisition time was approximately 10 h.

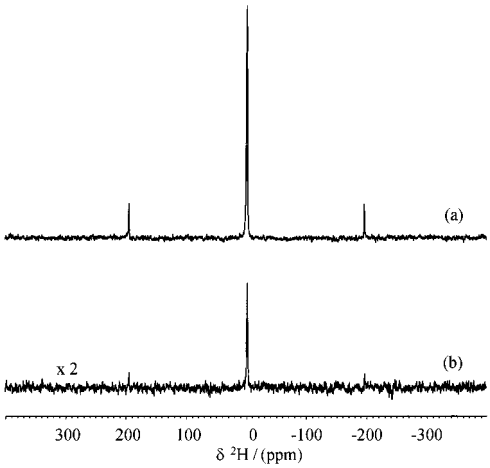

Figure 8. $^2H-\{^1H\}$ CPMAS spectra of TMC5-d_9 nonasil synthesized in (a) H_2O and (b) D_2O using a 200 μs contact time. Ninety-six scans were acquired and the intensity scale is the same for both spectra.

of 200 μs, consistent with the methyl deuterons interacting with the defect site. The results are *not* consistent with a physical model where the cyclopentyl ring is ordered toward the defect site. In that case, the signal at 10.5 ppm would likely not be present in the HETCOR spectrum at the contact time used. The results of the HETCOR experiment are consistent with a physical model where the methyl deuterons strongly interact with the defect site, suggesting that the charge centers are in close spatial proximity.

A sample of TMC5-d_9 nonasil was synthesized in D_2O to check our interpretation of the HETCOR results. Figure 8 shows $^2H-\{^1H\}$ CPMAS spectra of TMC5-d_9 nonasil samples synthesized in H_2O and D_2O at a contact time of 200 μs. The integrated spectral intensity of the sample made in D_2O is one-fourth that of the sample made in H_2O ($I^{CD_3}{}_{D_2O}/I^{CD_3}{}_{H_2O} = 0.24$). These results are consistent with the interpretation of the two-dimensional experiments showing that the silanol groups

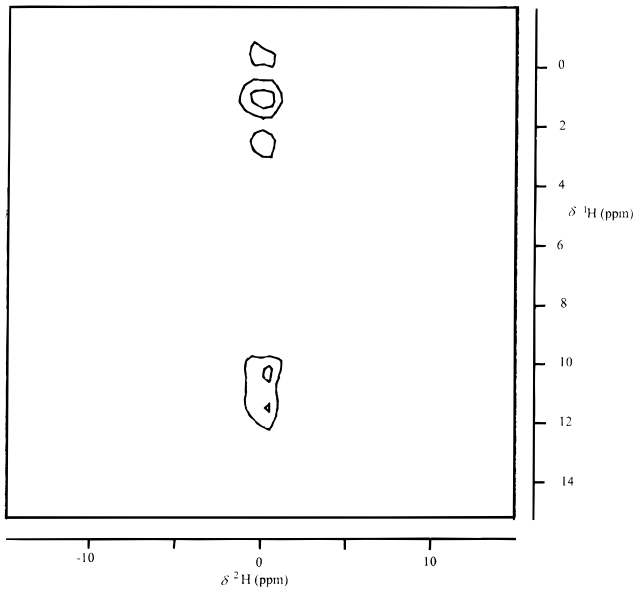

Figure 9. Two-dimensional $^2H-\{^1H\}$ CPMAS spectrum for TMC6-d_9 nonasil with a 200 μs contact time. Ninety-six scans were acquired for each experiment, a 20 Hz linebroadening was used in both dimensions, and the acquisition time was approximately 17 h.

of the defect site are *mostly responsible* for the magnetization transfer observed in the one-dimensional ^2H CPMAS spectrum. Again, these results are not consistent with the cyclopentyl ring being in close spatial proximity to the defect site. Also, the single pulse ^2H MAS spectrum of the sample made in D_2O (see the Supporting Information) has a line at -1.6 ppm due to the methyl deuterons ($\delta_{D_2O} = 0$ ppm) and a broader line at 5.8 ppm attributable to the silanols of the defect sites. However, only the resonance at -1.6 ppm is seen in the $^2H-\{^1H\}$ CPMAS spectrum at a 200 μs contact time, consistent with the conclusion that the methyl groups are between the defect silanols and the cyclopentyl ring. All of the above results suggest that the methyl deuterons are in closer spatial proximity to the defect site than the cyclopentyl ring.

The two-dimensional correlation spectrum for TMC6-d_9 nonasil is shown in Figure 9. Here two resonances are observed at 1.5 and 10.7 ppm. Again, the two-dimensional NMR results are consistent with the methyl deuterons strongly interacting with the defect site. A two-dimensional experiment was also ran on the TMC6-d_9 nonasil sample with a 100 μs contact time. The spectrum from that experiment (not shown) also exhibits the two resonances at 10.7 and 1.5 ppm, though the relative intensity of the resonance at 1.5 ppm is weaker than in the experiment with the 200 μs contact time. In the spectrum shown there are two weaker "lines" at -0.5 and 3.0 ppm. These are artifacts of the two-dimensional power mode Fourier transform. Two-dimensional experiments ran on both the TMC6 and TMC5 nonasil samples at long contact times (3 ms) do not show these peaks. Additionally, the signal-to-noise in the 2D spectra with longer contact times is much better. We believe these two extraneous peaks to be artifacts of spectral processing.

We recently reported a two-dimensional spectrum for the TMC6-d_9 nonasil sample which does not exhibit a resonance at 2 ppm.[27] The discrepancy is likely due to

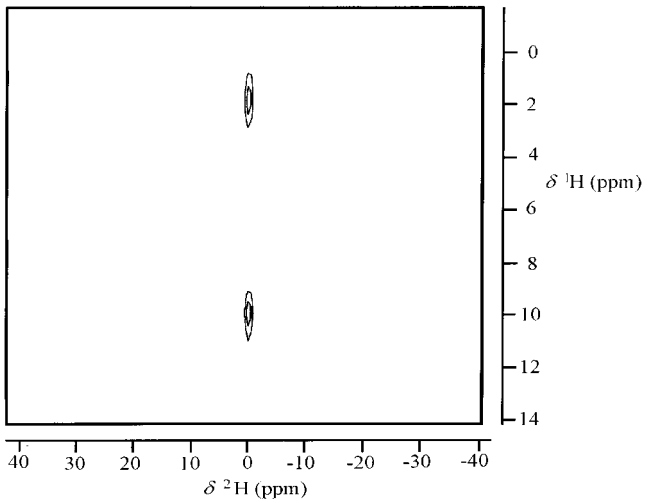

Figure 10. Two-dimensional $^2H-\{^1H\}$ CPMAS spectrum for SSZ-23-d_9 with a 200 μs contact time. One hundred and twenty-eight scans were acquired for each experiment, a 20 Hz line broadening was used in both dimensions, and the acquisition time was approximately 16 h.

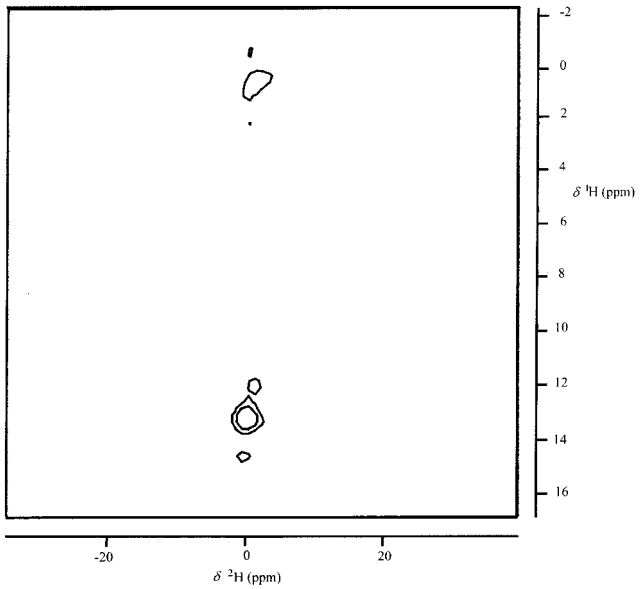

Figure 11. Two-dimensional $^2H-\{^1H\}$ CPMAS spectrum on ZSM-12-d_{12} with a 500 μs contact time. Two hundred and twelve scans were acquired per experiment, a 40 Hz line broadening was used in both dimensions, and the acquisition time was approximately 26 h. The two-dimensional spectrum shown was acquired using ^2H and ^1H rf field strengths of 59 and 50 kHz, respectively.

small errors in the pulse phases and amplitudes of the original experiments. The results presented here, however, are still consistent with the conclusions drawn from the original experiments. Extreme care must be taken when setting the pulse amplitudes and phases as the accumulation of small errors can result in the observation of artifacts in multidimensional spectra. For all multidimensional spectra presented here, the phases and amplitudes of the four pulses for both deuterium and hydrogen were checked and optimized immediately prior to the two-dimensional experiments.

SSZ-23. Figure 10 shows the results of the two-dimensional correlation experiments. Two signals are observed: one at 10.0 ppm due to the silanol groups in the defect site and one at 1.9 ppm due to the adamantane moiety. The average distance of the methyl group deuterons from the closest methylene protons is approximately 2.8 Å, with a closest distance of 2.0 Å. Again, the results suggest that the methyl groups are in close spatial proximity to the defect site. In contrast to the one-dimensional ^1H spectrum, the signal at 10 ppm in the two-dimensional spectrum is slightly stronger than the signal at 2 ppm. The adamantane moiety is rotating about its 3-fold symmetry axis, whereas the cyclic alkyl groups of the nonasil SDAs are essentially immobile.[7] While the effect of molecular motion on cross-polarization is difficult to quantify, clearly the silanols groups are involved in cross-polarization to the methyl deuterons. Again, we can conclude that there is spatial ordering of the SDA toward the defect site.

ZSM-12. The $^2H-\{^1H\}$ correlation spectrum for the ZSM-12 is shown in Figure 11. Due to the weak signal from the sample as discussed above, a contact time of 500 μs was used. As in the other three samples, two signals are observed in the correlation spectrum, one due to the silanols (13 ppm) in the defect site and one due to the protons on the SDA (1.4 ppm). The average distance of the methyl deuterons to the nearest methylene protons is approximately 2.4 Å. The deuterated methyl groups of this sample have four β methylene protons as compared to one for the nonasil sample (see Figure 1). Despite this, the relative intensity of the broad resonance at 13 ppm is stronger than the signal centered at 1.4 ppm.

For this sample, proton spin-diffusion is more pronounced than for the other materials, so stronger rf fields were used to increase the effective $T_{1\rho}$.[32] However, on the basis of ^1H two-dimensional experiments,[40] the resonance observed at 13 ppm is not due to proton spin-diffusion. Additionally, the HETCOR spectra using ^2H rf field strengths of 59 and 50 kHz are nearly identical. The results of the two-dimensional experiments suggest that the deuterons of the methyl groups are in close spatial proximity to the silanol groups of the defect site.

Viewed as a group, the results for all four as-made materials support a physical model where the charge center on the SDA is spatially ordered toward the charge-compensating defect site. The results seem to be general for all-silica materials, provided the charge is not in the center of the SDA, (i.e. TPA^+ cations) as this work encompasses a clathrasil, a one-dimensional large-pore zeolite (ZSM-12), and a small-pore multidimensional material (SSZ-23). Viewed in an alternative context, if the SDAs have some structural organization, i.e., in ZSM-12 the SDAs pack down the pore length single file, then this Coloumbic interaction should strongly influence the location of the charge-compensating defect site in the zeolite framework. This conclusion may have implications for the synthesis of aluminosilicates and metallosilicates made with cationic SDAs. For instance, if aluminum is incorporated in the zeolite framework near the charge on the SDA, the acid catalysis properties of a zeolite could in principle be tailored on the basis of the charge distribution of the SDA. The results presented here coupled with a detailed understanding of the mesoscopic organization

(40) Details of the ^1H spin-diffusion experiments and a thorough discussion of the results are given in ref 32.

of SDAs inside as-made materials could lead to better techniques for controlling the distribution of catalytic sites in zeolites on the basis of synthesis conditions.

Summary

The spatial ordering of the organic and inorganic charge centers in three as-made all-silica zeolites has been studied using NMR correlation spectroscopy. To the best of our knowledge this is the first study of its kind. The results for all three materials suggest a model where the charge centers are spatially ordered, with the deuterons on the methyl groups strongly interacting with the defect sites. We believe these results suggest an additional role for the SDA of influencing the location of defect sites in the framework of all-silica zeolites. This work also shows the importance of Coloumbic interactions in zeolite synthesis and structure-direction. In the case of aluminosilicates, it may be possible to influence the location of aluminum in the zeolite framework on the basis of the charge distribution of the SDA used. This could lead to tailoring the distribution of catalytic sites in zeolites on the basis of the charge distribution of the SDA.

Acknowledgment. This work was funded by NSF grant CTS-9713516. The authors thank the regents of the ACS-PRF for financial support, the Department of Chemistry and Biochemistry at the University of Delaware for use of the NMR facilities, and C. Dybowski, M. Bruch, and A. J. Vega for useful discussions.

Supporting Information Available: Static ^{2}H NMR, ^{2}H−{^{1}H} MAS, ^{2}H MAS, and ^{2}H−{^{1}H} CPMAS spectra of compounds examined in this paper (6 pages). Ordering information is given on any current masthead page.

CM9804517